Brief Communication

Cell Chemical Biology

An antisense transcript transcribed from *Irs2* locus contributes to the pathogenesis of hepatic steatosis in insulin resistance

Graphical abstract

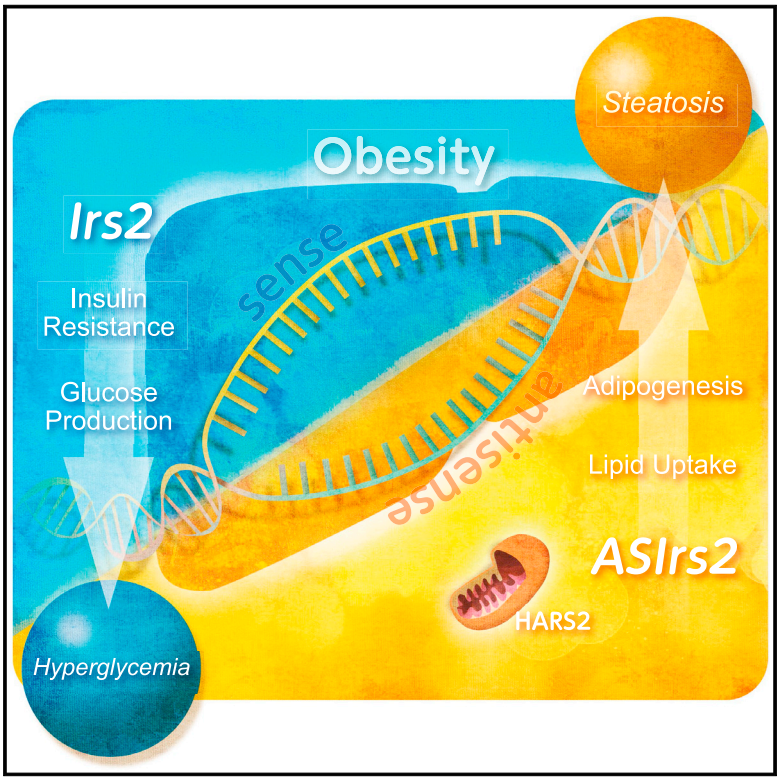

Authors

Maya Matsushita, Motoharu Awazawa, Naoki Kobayashi, ..., Matthias Blüher, Jens C. Brüning, Kohjiro Ueki

Correspondence

mawazawa@ri.ncgm.go.jp (M.A.), uekik@ri.ncgm.go.jp (K.U.)

In brief

Although insulin resistance and steatosis are known to be associated through upregulation of lipogenic genes in liver, the underlying mechanism remains unclear. Here, Matsushita et al. show that *Irs2* and its natural antisense transcript *ASIrs2* are reciprocally regulated in insulin-resistant liver, thus causing insulin resistance and lipid accumulation, respectively.

Highlights

- *ASIrs2* is a natural antisense transcript of *Irs2*
- Liver *ASIrs2* and *Irs2* are reciprocally regulated in different nutritional conditions
- ASIrs2 suppression ameliorates steatosis with PPARγ suppression
- HARS2 is a possible binding protein of *ASIrs2* mediating its adipogenic function

Matsushita et al., 2022, Cell Chemical Biology *29*, 680–689
April 21, 2022
https://doi.org/10.1016/j.chembiol.2021.12.008

CellPress

CellPress

Cell Chemical Biology

Brief Communication

An antisense transcript transcribed from *Irs2* locus contributes to the pathogenesis of hepatic steatosis in insulin resistance

Maya Matsushita,[1] Motoharu Awazawa,[1,11,*] Naoki Kobayashi,[1] Yoshiko Matsumoto Ikushima,[1] Kotaro Soeda,[1] Miwa Tamura-Nakano,[1] Masafumi Muratani,[2] Kenta Kobayashi,[3] Matthias Blüher,[4,5] Jens C. Brüning,[6,7,8,9] and Kohjiro Ueki[1,10,*]

[1]Department of Molecular Diabetic Medicine, Diabetes Research Center, Research Institute, National Center for Global Health and Medicine, 1-21-1 Toyama, Shinjuku, Tokyo 162–8655, Japan
[2]Department of Genome Biology, Faculty of Medicine, University of Tsukuba, 1-1-1 Tennodai, Tsukuba, Ibaraki 305-8575, Japan
[3]Section of Viral Vector Development, National Institute for Physiological Sciences, Hojozaka 27, Myodaiji, Okazaki, Aichi 305-8575, Japan
[4]Medical Department III–Endocrinology, Nephrology, Rheumatology, University of Leipzig, Leipzig, Germany
[5]Helmholtz Institute for Metabolic, Obesity and Vascular Research (HI-MAG) of the Helmholtz Zentrum München, University of Leipzig and University Hospital Leipzig, Leipzig, Germany
[6]Department of Neuronal Control of Metabolism, Max Planck Institute for Metabolism Research, Gleueler Strasse 50, 50931 Cologne, Germany
[7]Center for Endocrinology, Diabetes and Preventive Medicine (CEDP), University Hospital Cologne, Kerpener Strasse 26, 50924 Cologne, Germany
[8]Excellence Cluster on Cellular Stress Responses in Aging Associated Diseases (CECAD) and Center for Molecular Medicine Cologne (CMMC), University of Cologne, Joseph-Stelzmann Strasse 26, 50931 Cologne, Germany
[9]National Center for Diabetes Research (DZD), Ingolstädter Landstrasse 1, 85764 Neuherberg, Germany
[10]Department of Molecular Diabetology, Graduate School of Medicine, The University of Tokyo, 3-7-1 Hongo, Bunkyo-Ku, Tokyo 113-8655, Japan
[11]Lead contact
*Correspondence: mawazawa@ri.ncgm.go.jp (M.A.), uekik@ri.ncgm.go.jp (K.U.)
https://doi.org/10.1016/j.chembiol.2021.12.008

SUMMARY

During insulin resistance, lipid uptake by the liver is promoted by peroxisome proliferator-activated protein (PPAR) γ upregulation, leading to hepatic steatosis. Insulin, however, does not directly regulate adipogenic gene expression in liver, and the mechanisms for its upregulation in obesity remain unclear. Here, we show that the *Irs2* locus, a critical regulator of insulin actions, encodes an antisense transcript, *ASIrs2*, whose expression increases in obesity or after refeeding in liver, reciprocal to that of *Irs2*. *ASIrs2* regulates hepatic *Pparg* expression, and its suppression ameliorates steatosis in obese mice. The human ortholog *AL162497.1*, whose expression is correlated with that of hepatic *PPARG* and the severity of non-alcoholic steatohepatitis (NASH), shows genomic organization similar to that of *ASIrs2*. We also identified HARS2 as a potential binding protein for *ASIrs2*, functioning as a regulator of *Pparg*. Collectively, our data reveal a functional duality of the *Irs2* gene locus, where reciprocal changes of *Irs2* and *ASIrs2* in obesity cause insulin resistance and steatosis.

INTRODUCTION

Due to pervasive transcription throughout the mammalian genome (Consortium et al., 2012), transcripts are often produced from the opposite strand of a given gene locus, and these are called natural antisense transcripts (NATs) (Pelechano and Steinmetz, 2013). Current estimations indicate that 30% and 90% of coding genes have NATs in humans and in mice, respectively (Ozsolak et al., 2010). Recent reports demonstrate close correlations between the expression levels of NATs and those of their counterpart transcripts, suggestive of their functional coordination (Katayama et al., 2005). Insulin signaling plays a central role in the physiological regulation of metabolism, while its dysregulation causes insulin resistance. Given the prevalence of antisense transcription, it is assumed that a significant proportion of insulin-signaling molecules have NATs, whose significance in insulin actions and metabolism, however, has not been systematically investigated. Here, we show that from the locus of *Irs2*, one of the crucial determinants of insulin actions, a NAT, *9530052E02Rik* (termed hereafter as *ASIrs2*), is transcribed, whose expression is altered in a manner strikingly reciprocal to that of *Irs2*. *ASIrs2* suppression led to reduced *Pparg* in liver, with amelioration of steatosis in obese mice. The human *IRS2* locus encodes an antisense transcript with a genomic orientation similar to that of *ASIrs2* in mice and whose expression was correlated with *PPARG* and the severity of non-alcoholic steatohepatitis (NASH). Collectively, our data suggest a mechanism explaining the concurrent occurrence of insulin resistance and fatty liver under obesity through reciprocal changes of *Irs2* and *ASIrs2*.

CellPress

A

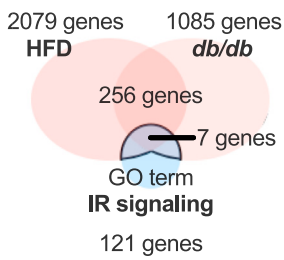

B

Sense	NCD (Cts)	HFD (Cts)	FC	FDR	misty (Cts)	db/db (Cts)	FC	FDR	Antisense
Enho	132.9	9.9	−11	1.6E−16	34.3	2	−14.6	5.9E−18	*Dnaic1, Gm12405, Gm12406*
Igf2	ND	ND	–	–	3.1	10.3	3.3	1.3E−02	*Igf2os*
Irs2	1008.9	302.4	−3.6	1.7E−09	709.8	116.8	−6.1	8.0E−27	*9530052E02Rik*
Mup1	5485.5	26.6	−199.2	3.3E−247	2879.7	168	−16.7	1.0E−168	*Dpp6*
Nucb2	ND	ND	–	–	33.8	9.8	−3.3	3.3E−08	–
Pak1	14.2	61.5	5.83	2.3E−23	ND	ND	–	–	–
Serpina12	ND	ND	–	–	222.8	28.1	−7.9	4.7E−66	–

C

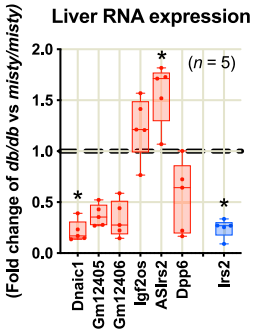

D

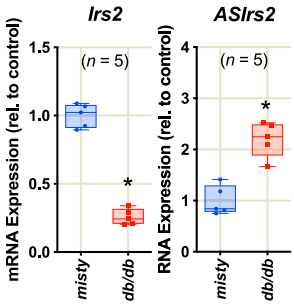

E

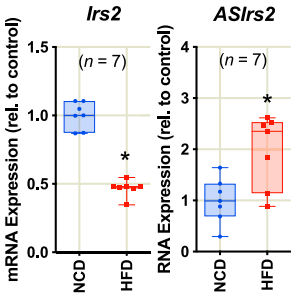

F

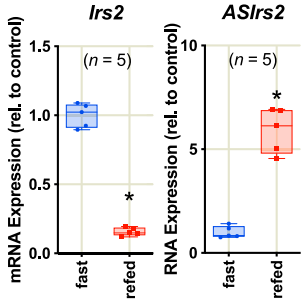

G

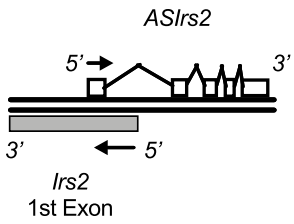

H

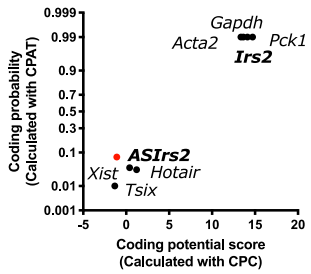

I

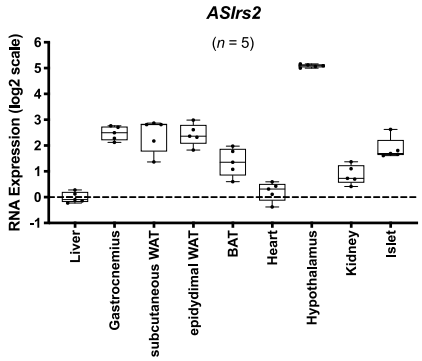

J

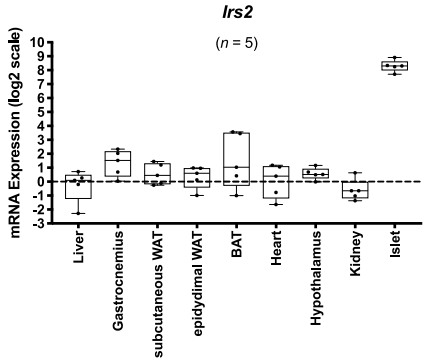

H

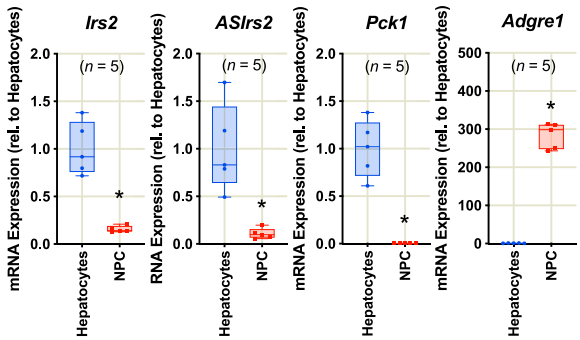

L

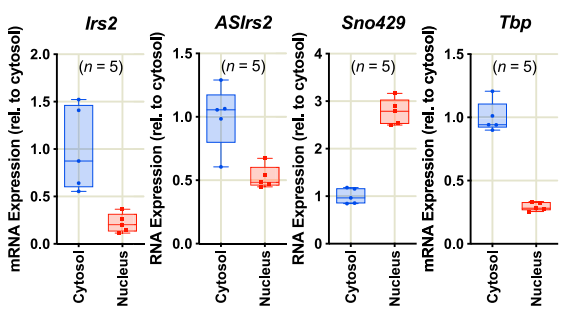

(legend on next page)

RESULTS

ASIrs2 and *Irs2* transcripts exhibit discordant expression patterns in liver

An evolutionary model suggests that functional non-coding RNAs (ncRNAs) likely have close relations with their nearby protein-coding genes in their expression (Palazzo and Koonin, 2020) as well as in their functions (Katayama et al., 2005). On the basis of these assumptions, we expected to identify NATs with metabolic functions by screening insulin-signaling-related genes that undergo transcriptional regulation. We used RNA-sequencing (RNA-seq) analyses to screen for the genes undergoing transcriptional changes either in the liver of high-fat-diet (HFD)-induced obese mice or in the liver of *Lepr*-deficient *db*/*db* mice compared with the livers of the respective control mice (false discovery rate [FDR] < 0.05). Whereas lipid-metabolism-related genes showed a general trend of transcriptional regulation (Figures S1A and S1B), only seven genes showed altered transcript levels in the obese-liver samples with the gene ontology (GO) term ''insulin receptor (IR) signaling pathway'' (Figure 1A), among which four genes harbored at least one NAT (Figure 1B). NAT *9530052E02Rik*, a previously uncharacterized NAT in the *Irs2* locus (*ASIrs2*), had a unique expression pattern showing significant upregulation in *db*/*db* mouse liver compared with the controls (Figure 1C), reciprocal to that of *Irs2* (Figure 1D). *ASIrs2* expression was ~1,000 times lower compared with *Irs2* (Figure S1C), consistent with the general characteristics of NATs (Pelechano and Steinmetz, 2013). *ASIrs2* and *Irs2* were also reciprocally regulated between the livers of lean normal-chow-diet (NCD)-fed mice and those of HFD-induced obese mice (Figure 1E) or between the livers of fasted and refed mice (Figure 1F). *ASIrs2* was located in a head-to-head orientation to *Irs2* (Figures 1G and S1D) and lacked canonical coding potential (Figure 1H). *ASIrs2* showed ubiquitous expression in insulin target tissues (Figure 1I), the pattern of which was, unlike that in liver, not entirely reciprocal to that of *Irs2* (Figure 1J). In liver, *ASIrs2* was predominantly expressed in the hepatocyte fraction (Figure 1K), with relatively high levels of transcripts localizing in the cytoplasm, as assessed by subcellular fractionation (Figure 1L).

ASIrs2 suppression reduced *Pparg* expression in wild-type mouse liver in the postprandial state

Irs2 is one of the essential components of insulin signaling in liver and undergoes dynamic transcriptional regulation with feeding status (Kubota et al., 2008), while its reduction in obesity causes insulin resistance (Shimomura et al., 2000). In order to test if *ASIrs2* could also have metabolic functions in liver, we conducted adeno-associated virus (AAV)-mediated delivery of short hairpin RNA (shRNA) targeting *ASIrs2* (shASIrs2) (Figure 2A). Blunted induction of *ASIrs2* in wild-type mouse liver after refeeding (Figures 2B and S1E) led to no alterations in body weight (Figure 2C), blood glucose or insulin levels (Figures 2D and 2E), or liver weights (Figure 2F). Although accumulating evidence demonstrates the ''sense'' counterpart gene regulation by NATs (Faghihi and Wahlestedt, 2009), we found no differences in the IRS2 levels (Figures 2G and 2H), in phospho-Akt levels (Figures S1F and S1G) or in gluconeogenic gene expression (Figure S1H) between the two AAV injections.

In order to unbiasedly assess the impact of *ASIrs2* suppression on liver, we investigated the transcriptomes of the liver of mice administered control or shASIrs2 AAV in the refed condition. The analyses revealed 102 upregulated and 224 downregulated genes in the liver of shASIrs2 AAV-administered mice compared with those of controls (FDR < 0.05; Table S1). Whereas no gene sets were enriched in the upregulated genes, the ''peroxisome'' gene set was identified by gene set enrichment analysis (GSEA) as the only enriched category in the significantly downregulated genes (Figures 2I and 2J), with DAVID functional annotation analysis (Dennis et al., 2003) showing enrichment of lipid-metabolism-related genes in the significantly downregulated genes in the shASIrs2-AAV-administered mouse liver (Figure 2K). Among the genes known to play regulatory roles in lipid metabolism (Jump et al., 2005), *Pparg* expression was significantly lower in the liver of the shASIrs2-AAV-treated mouse than in the control (Figure 2L), as was confirmed by real-time PCR analyses (Figure 2M), which also showed that *Pparg1* was significantly reduced, while *Pparg2* also tended to be reduced (Figure S1I). Suppression of *ASIrs2* in Hepa 1-6 hepatoma cells with siRNA (Figure 2N) or locked nucleic acid (LNA) (Figure 2O) also lowered *Pparg* expression, indicating that *ASIrs2* suppression impinged on *Pparg* expression in a cell-autonomous manner. A luciferase assay using 3.1 kb of the 5′ flanking region of *Pparg1* failed to show changes of promoter activity by *ASIrs2* suppression (Figure S1J). Collectively, these data suggested that *ASIrs2* suppression impinged on the expression of lipid-metabolism-related genes with reduced *Pparg* in hepatocytes.

On the other hand, *ASIrs2* suppression *in vivo* led to no alteration of *Ppara* (Figure S1K), nor did it affect oxygen consumption rates *in vitro* (Figure S1L), suggesting that *ASIrs2* suppression did not interfere with β-oxidation.

Figure 1. *ASIrs2* and *Irs2* transcripts exhibit discordant expression patterns in liver

(A) A Venn diagram showing the strategy to select seven IR signaling-related genes with transcriptional regulation.

(B) The read counts (Cts) and relative gene expression from RNA-seq analysis in liver and their corresponding NATs. FC HFD, fold change of HFD-fed mice compared with controls; FC db, fold change of *db*/*db* compared with *misty*/*misty* mice (n = 4).

(C) The relative expression of NATs and *Irs2* in *db*/*db* mouse liver compared with the controls.

(D–F) The relative expression of *Irs2* and *ASIrs2* in *db*/*db* mouse liver compared with the controls (D), in HFD-fed mouse liver compared with the controls (E), and in the liver of wild-type mice after 6 h of refeeding (refed) compared with that in the fasted condition (F).

(G) Genomic organization of *ASIrs2* and *Irs2*.

(H) Coding potential by CPAT and CPC.

(I and J) The relative expression of *ASIrs2* (I) and *Irs2* (J) in different insulin target tissues. WAT, white adipose tissue; BAT, brown adipose tissue.

(K) The relative gene expression in the hepatocytes and non-parenchymal cells (NPC) fractionated from wild-type mouse liver.

(L) The relative gene expression in the cytosolic and nuclear fractions of purified hepatocytes from wild-type mouse. *p < 0.05 using unpaired, two-tailed Student's t test, corrected for multiple comparisons with the Holm-Sidak method when applicable. Box-and-whisker plots represent 25th and 75th percentiles, the median, the minimum-to-maximum values, and the individual data points. See also Figure S1.

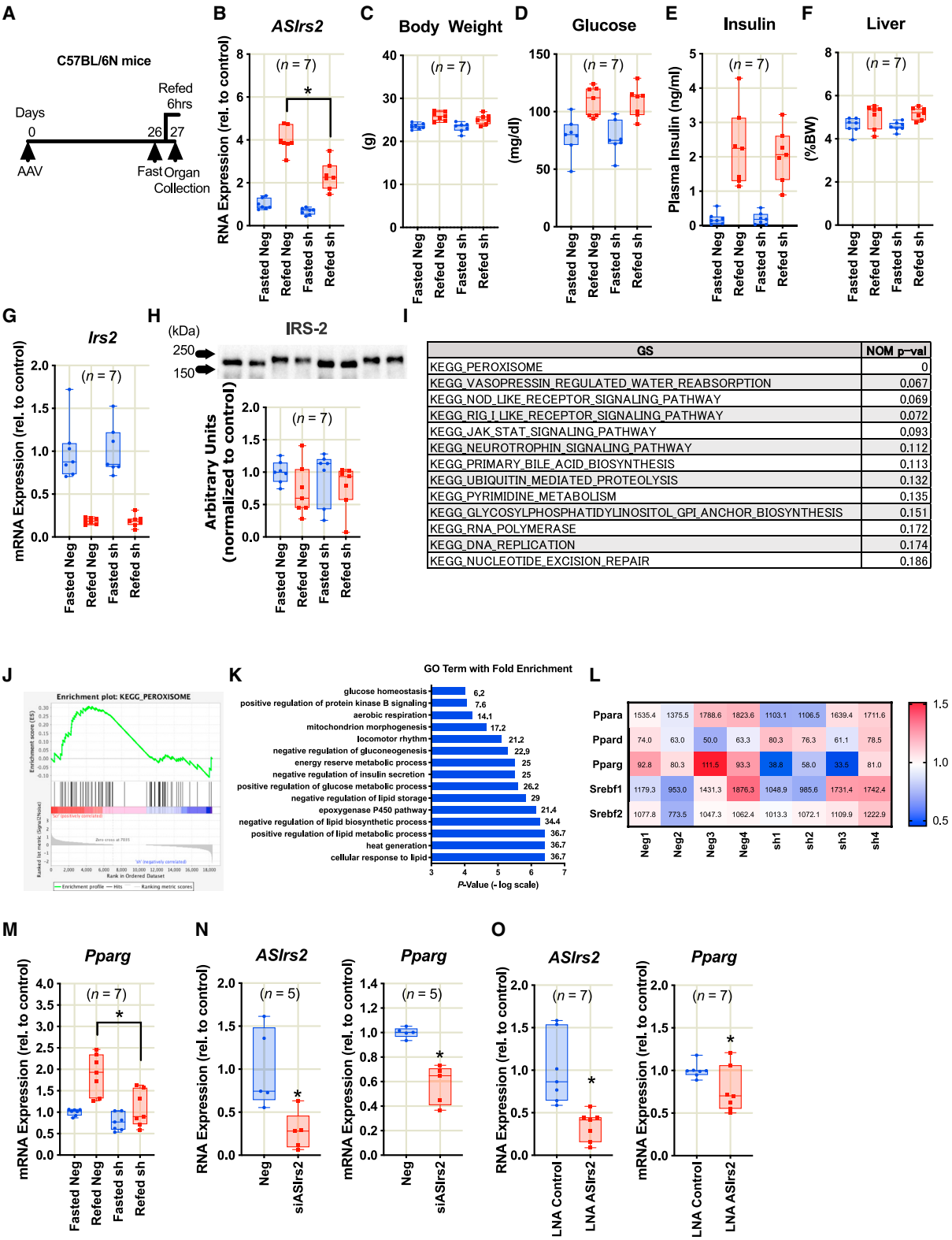

GS	NOM p-val
KEGG_PEROXISOME	0
KEGG_VASOPRESSIN_REGULATED_WATER_REABSORPTION	0.067
KEGG_NOD_LIKE_RECEPTOR_SIGNALING_PATHWAY	0.069
KEGG_RIG_I_LIKE_RECEPTOR_SIGNALING_PATHWAY	0.072
KEGG_JAK_STAT_SIGNALING_PATHWAY	0.093
KEGG_NEUROTROPHIN_SIGNALING_PATHWAY	0.112
KEGG_PRIMARY_BILE_ACID_BIOSYNTHESIS	0.113
KEGG_UBIQUITIN_MEDIATED_PROTEOLYSIS	0.132
KEGG_PYRIMIDINE_METABOLISM	0.135
KEGG_GLYCOSYLPHOSPHATIDYLINOSITOL_GPI_ANCHOR_BIOSYNTHESIS	0.151
KEGG_RNA_POLYMERASE	0.172
KEGG_DNA_REPLICATION	0.174
KEGG_NUCLEOTIDE_EXCISION_REPAIR	0.186

Figure 2. *ASIrs2* suppression reduced *Pparg* expression in wild-type mouse liver in the postprandial state

(A) A schema of the *ASIrs2* knockdown experiment.

(B–H) The relative expression of ASIrs2 in liver (B); the body weights (C), blood glucose levels (D), plasma insulin levels (E), and liver weights (F); the relative expression of *Irs2* in liver (G); and a representative blot with the relative quantification of IRS-2 protein in liver (H) of the mice administered shASIrs2 (sh) or negative-control AAV (Neg).

(legend continued on next page)

ASIrs2 in obese mice or *AL162497.1* in humans and their significance in steatosis

Given these data, we hypothesized that hepatic *ASIrs2* upregulation in obese insulin-resistant mice could induce *Pparg* and promote steatosis. Indeed, *Pparg* expression was positively correlated with *ASIrs2* expression in the pooled liver samples from mouse models with different degrees of obesity (Figure 3A). Thus, we suppressed *ASIrs2* in the liver of *db/db* mice with shASIrs2-AAV administration (Figure 3B), which led to a significant reduction of *ASIrs2* only in liver compared with the controls (Figures 3C and S2A). Although no differences were observed between the groups in their body weights (Figure 3D), *Pparg* expression was significantly lower in the liver of shASIrs2-AAV-administered *db/db* mice than in that of controls (Figures 3E and S2B), as well as that of genes involved in hepatic lipid uptake (Figures 3F–3K), whereas that of *Srebf1* (Figure 3L) and *Ppara* (Figure 3M) remained unaltered (Lee et al., 2018) (Figures 3F–3M). The *miR-122* expression was not affected by shASIrs2 administration (Figure 3N), excluding the possibility of liver toxicity by shRNA-conveying AAV (Grimm et al., 2006). ASIrs2 suppression led to significantly reduced liver weight compared with the controls (Figure 3O), which was associated with lower liver triglyceride (TG) content (Figure 3P), as was confirmed by liver oil red O staining (Figure 3Q), almost to the levels of control lean mice.

Whereas an insulin tolerance test did not reveal differences in their glucose levels (Figure S2C), a glucose tolerance test showed, despite the amelioration of steatosis, higher glucose levels in shASIrs2-AAV-administered *db/db* mice than in the controls (Figures S2D and S2E), with comparable levels of plasma insulin levels (Figure S2F) or of gluconeogenic gene expression in liver (Figure S2G). These results were consistent with the previous report describing exacerbation of glucose intolerance in PPARγ-abrogated leptin-deficient mice, possibly due to insulin resistance in muscles and white adipose tissues (Matsusue et al., 2003). Kupffer cells did not express detectable amounts of *ASIrs2* (Figure S2H), with *Pparg* remaining unaltered upon shASIrs2-AAV administration (Figure S2I), suggesting that the possible increment of Kupffer cells for the observed metabolic phenotypes was unlikely (Moran-Salvador et al., 2011). Collectively, these data indicated that the increased hepatic *ASIrs2* in obesity could contribute to the pathogenesis of steatosis in mice.

In humans, the locus of the *IRS2* gene encodes NAT *AL162497.1*, and although its sequence similarity with *ASIrs2* is 38% and low, its geographic orientation to *IRS2* is conserved compared with that of *ASIrs2* to *Irs2* in mouse (Figures S3A and S3B). Assessment by GTEx showed low but ubiquitous expression of *AL162497.1* among tissues (Figure S3C), which was, like *ASIrs2* and *Irs2* in mouse, not reciprocal with that of *IRS2* (Figure S3D). Analyses of human liver (Table S2) showed that the expression of *AL162497.1* was significantly correlated with the visceral fat area (Figure 3R) but not with the subcutaneous fat area (Figure S3E). *PPARG* expression was positively correlated with that of *AL162497.1* (Figure 3S), and *AL162497.1* expression was higher in the human subject with higher NASH scores (Figure 3T), similar to the expression levels of *PPARG* (Figures S3F and S3G). *AL162497.1* expression was positively correlated with that of *TGFB1* as a marker of fibrosis (Figure S3H), whereas no positive correlations were observed with those of *SREBF1*, *SCD*, and *PPARA* (Figures S3I and S3K) or with fasting plasma insulin levels and homeostasis model assessment of insulin resistance (HOMA-IR) (Figure S3L). These data were consistent with the possibility that *AL162497.1* in humans could contribute to the pathogenesis of NASH in a manner analogous to that of *ASIrs2* in mouse. Interestingly, at least in our cohort, no negative correlation was observed between the expression of *IRS2* and the levels of visceral fat area (Figure S3M) or that of *AL162497.1* (Figure S3N), suggesting the existence of independent regulatory mechanisms for *IRS2* and *AL162497.1* expression.

ASIrs2 is bound to HARS2, the suppression of which increased hepatic *Pparg in vitro* and *in vivo*

Next, we explored the mechanism of adipogenic gene expression by *ASIrs2* in liver. The predicted 2D structure of *ASIrs2* showed a stem-loop formation, typical of a non-coding RNA interacting with a protein (Huang et al., 2018; Xia et al., 2018) (Figure S4A). To identify potential binding proteins of *ASIrs2*, we conducted a pull-down assay by labeled *ASIrs2*, using liver lysates prepared from two independent wild-type mice. Unbiased proteome analyses of the precipitated proteins detected 2,462 proteins. The enrichment ratios of the amount precipitated by *ASIrs2* to that precipitated by negative control RNA from the two liver samples showed high correlation (Figure 4A). Interestingly, many of the genes in *ASIrs2*-precipitated proteins were those localized in mitochondria (Figure 4B). Among the four proteins with highest enrichments was the mitochondrial aminoacyl-tRNA synthetase *Hars2*, followed by *Tsn/Tsnax* complex and *Cnbp*, the last three of which are all transcription factors (Figure 4C). Indeed, a substantial proportion of *ASIrs2* was detected in the mitochondrial fraction of mouse liver (Figure 4D), suggesting *ASIrs2* localization in mitochondria. When we overexpressed FLAG-tagged *Hars2*, *Tsn*, or *Cnbp* together with *ASIrs2* in Hepa 1-6 cells and performed an RNA-immunoprecipitation (RIP) assay, HARS2 overexpression exclusively precipitated *ASIrs2*, indicating that HARS2 could serve as a binding protein for *ASIrs2* (Figure 4E). Prediction by an RNA-protein interaction prediction algorithm (RPIseq; Muppirala et al., 2011) also showed a high probability of interaction between HARS2 and *ASIrs2*, with the region spanning a relatively large proportion, 290–735 bp, suggesting it is required for the interaction (Figure S4B).

Hars2 is a mitochondrial histidyl-tRNA synthetase and is known as a causal gene for Perrault syndrome (Newman et al., 1993),

(I–K) The gene sets (GS) with nominal p values (NOM p-val) by GSEA based on the KEGG pathway database (I) with the enrichment plot of the peroxisome pathway (J) and DAVID functional annotation analyses (FDR < 0.05) (K) of the significantly downregulated genes in shASIrs2 AAV-administered mouse liver. KEGG, Kyoto Encyclopedia of Genes and Genomes.

(L) The relative expressions of indicated genes with read counts in the transcriptome analysis. The columns represent each experimental animal.

(M) The relative expression of *Pparg* in liver.

(N and O) The relative expression of *ASIrs2* and *Pparg* in Hepa 1-6 cells transfected with siRNA for *ASIrs2* (siASIrs2) or negative-control siRNA (Neg) (N) or with LNA for *ASIrs2* (LNA ASIrs2) or negative control (LNA Control) (O). *p < 0.05 using one-way ANOVA with the Holm-Sidak multiple comparison test, except for (N) and (O), where two-tailed Student's t test was applied. For explanation of boxplots see Figure 1 legend. See also Figure S1 and Table S1.

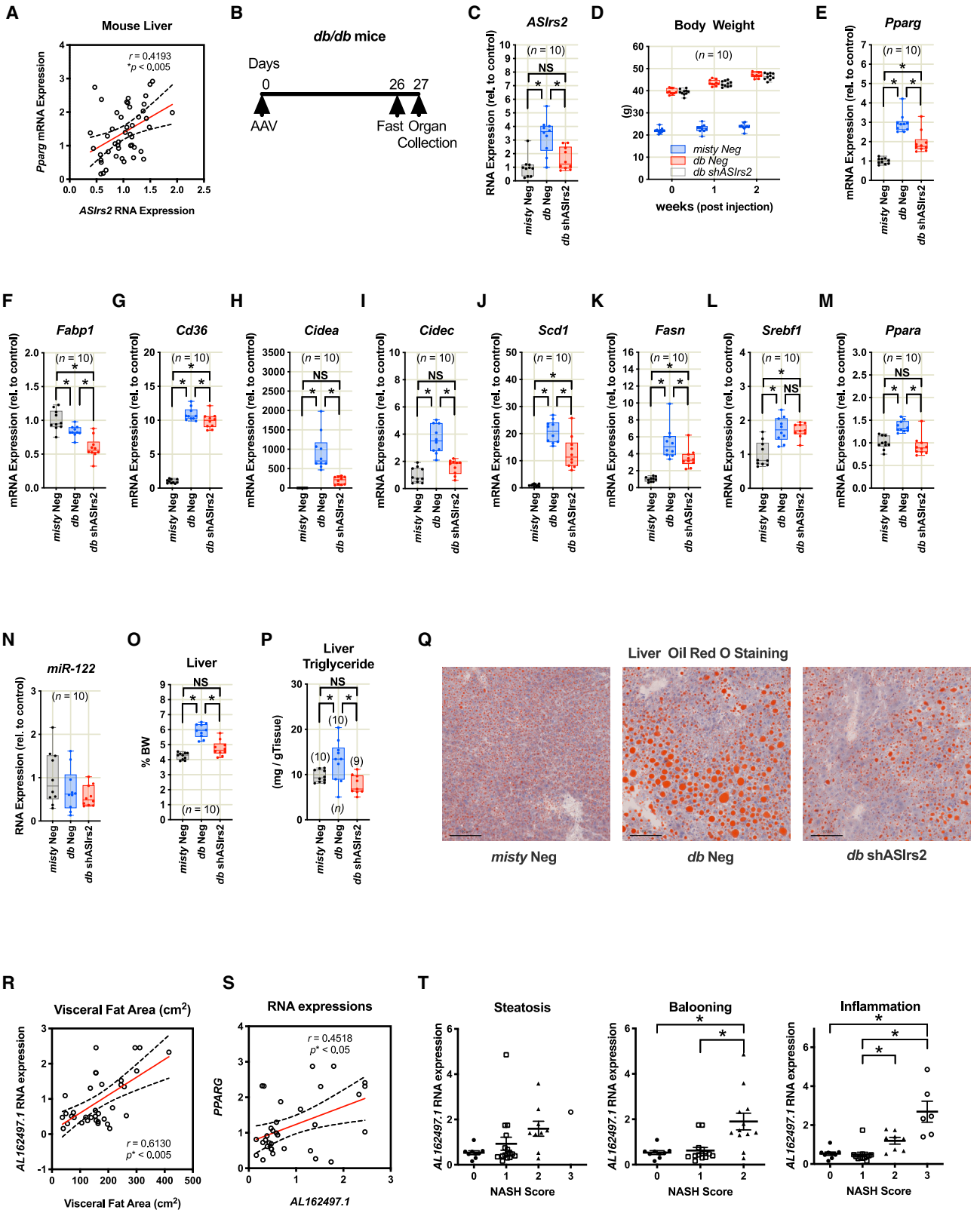

(legend on next page)

although the metabolic manifestations of it have not been well documented, nor the precise mechanisms whereby the genetic mutations lead to the syndrome (Gispert et al., 2013). In order to determine the roles of HARS2 in hepatic lipid metabolism, we suppressed hepatic *Hars2* expression via AAV (shHars2) in mouse liver in combination with short-term HFD feeding (Figure 4F). Although body weights did not differ between the shHars2-AAV-injected and the control shLacZ-AAV-injected mice (Figure 4G), *Pparg* expression was significantly higher in the shHars2-AAV-injected mice compared with the controls, with a tendency of a higher expression level of *Cd36* (Figure S4C), whereas *Ppara* and *Srebf1* expression was unaltered (Figure 4H). The liver weight of shHars2-AAV-injected mice was higher than that of controls, with more prominent lipid deposition being observed by histological examination (Figure 4I), suggesting acceleration of steatosis by *Hars2* suppression. SiRNA-mediated suppression of *Hars2* also led to upregulation of *Pparg* in Hepa 1-6 cells (Figure 4J). These data suggested that the loss of function of *Hars2* could lead to *Pparg* upregulation in hepatocytes. Of note, whereas liver *Hars2* mRNA expression was comparable between *db*/*db* mice and the lean control mice (Figure S4D), *HARS2* mRNA expression in human liver samples was, unexpectedly, correlated positively with *AL162497.1* (Figure S4E), implying its possible roles in hepatic metabolism in humans.

DISCUSSION

During insulin-resistant states, insulin is paradoxically capable of enhancing *de novo* lipogenesis in liver, promoting fatty liver changes (Brown and Goldstein, 2008). *De novo* lipid synthesis, however, contributes to only 26% of the liver TG, at least in human steatosis (Donnelly et al., 2005), highlighting the importance of lipid uptake from food and insulin-resistant adipose tissues. In fatty liver disease, a set of genes involved in lipid uptake or in lipid storage is upregulated with the increase and activation of PPARγ, contributing to its pathogenesis (Wang et al., 2020). To date, however, direct mechanisms have not been identified as to how the attenuation of insulin signaling could be reflected on coordinated enhancement of lipid uptake by liver under insulin-resistant states. Our results suggest that the reduced *Irs2* expression, one of the hallmarks of insulin resistance, was concomitantly associated with high *ASIrs2* expression, whereby fat accumulation is promoted with lipogenic gene induction, including PPARγ. These findings characterizing ncRNA-mediated regulation of metabolism propose a model that could unitarily explain the concurrent occurrence of insulin resistance and fatty liver under obesity through reciprocal regulation of two transcripts from the *Irs2* locus.

The regulatory mechanism for *ASIrs2* expression is yet to be determined. However, in the case of genes oriented in a head-to-head manner, the transcription of either gene could prevent the transcription of the opposite gene (“transcriptional collision”) (Faghihi and Wahlestedt, 2009), explaining well the reciprocal regulation of *ASIrs2* and *Irs2* in liver. On the other hand, the expression of *ASIrs2* and *Irs2* was not entirely reciprocal, for instance, in the tissue distribution in mice, similar to that of *AL162497.1* and *IRS2*. Of note, NATs could also be regulated through their own promoter activity (Lin et al., 2015), and these two modes of regulation would not be mutually exclusive. The transcriptional collision model would well explain their reciprocal regulation under different nutritional statuses, while their respective regulation could overlay their expression patterns.

Our results suggest that *ASIrs2* increases in liver in response to feeding and induces *Pparg* expression. Although it would be plausible that PPARγ could play a role in lipid storage in physiological postprandial status, to which *ASIrs2* upregulation could contribute, it is controversial whether *Pparg* is indeed induced in liver after feeding (Kubota et al., 2016; Matsuo et al., 2017). These discrepancies in currently available reports could have derived from the conditions of the feeding schemes or the age of the mice, while the exact significance of PPARγ and *ASIrs2* in the postprandial status remains to be further characterized.

Our assessments imply the possibility that *ASIrs2* hinders the function of HARS2 and thus upregulates *Pparg*. Such a possible signaling path from nucleus to mitochondria mediated by an ncRNA has been already suggested (Mercer et al., 2011; Noh et al., 2016). The complete nature of the *ASIrs2*/HARS2 interaction and functions is yet to be elucidated. Our promoter analyses did not show changes in *Pparg1* promoter activity upon *ASIrs2* suppression, while we could not exclude the possibility that the region we adopted here was insufficient for the effects of *ASIrs2*. Interestingly, numerous moonlighting functions have been reported for aminoacyl-tRNA synthetases (Guo and Schimmel, 2013), including mitochondrial aminoacyl-tRNA (Wang et al., 2016). Our results also suggest HARS2 could have unique roles in liver lipid metabolism, offering HARS2 as a fascinating target for future research.

There are some limitations in our assays that identified and characterized HARS2. First, our fractionation assay did not distinguish those merely attached to mitochondria from those within mitochondria (mitoplast). Especially given that *Hars2* is not mitochondrial but is nuclear encoded, we cannot exclude the possibility

Figure 3. *ASIrs2* in obese mice or *AL162497.1* expression in humans and their significance in steatosis

(A) A scatterplot of *ASIrs2* and *Pparg* expression in pooled liver samples.

(B) A schema of the *ASIrs2* knockdown experiment.

(C–Q) The relative expression of *ASIrs2* in liver (C), the body weights (D), the relative gene expression in the liver (E, *Pparg*; F, *Fabp1*; G, *Cd36*; H, *Cidea*; I, *Cidec*; J, *Scd1*; K, *Fasn*; L, *Srebf1*; M, *Ppara*; N, *miR-122*), the liver weights (O), and the liver triglyceride contents (P), with the representative oil red O-stained images of liver sections (Q) of *misty*/*misty* mice and *db*/*db* mice administered negative control AAV (*misty* Neg and *db* Neg) or *db*/*db* mice administered shASIrs2 AAV (*db* shASIrs2).

(R–T) The analyses of human liver samples. The correlations of liver *AL162497.1* expression with visceral fat area (n = 35) (R), the correlations of *PPARG* expression with *AL162497.1* in liver (n = 33) (S), and the expression of liver AL162497.1 in individuals with respective NASH scores as indicated (n = 35) (T). NS, not significant. *p < 0.05 using one-way ANOVA with the Holm-Sidak multiple comparison test, except for (A), (R), and (S), where the Pearson correlation was applied, and for (T), where the Kruskal-Wallis test with Dunn’s multiple comparison correction was applied, as distribution normality was not verified with the D’Agostino-Pearson test. In (A), (R), and (S), linear regression with 95% confidential interval bands is shown. In (T), the graphs represent mean ± SEM. For explanation of boxplots see Figure 1 legend. See also Figures S2, S3, and Table S2.

CellPress

A

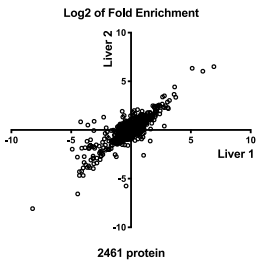

B

Term	%	P-Value	Benjamini
intracellular ribonucleoprotein complex	19.6	4.8E-07	3.1E-05
mitochondrion	34.8	2.5E-06	8.1E-05
nucleoplasm	28.3	8.4E-04	1.8E-02
nuclear speck	10.9	1.1E-03	1.8E-02
mitochondrial inner membrane	13	1.7E-03	2.1E-02
spliceosomal complex	8.7	3.5E-03	3.7E-02
nucleus	45.7	2.7E-02	2.2E-01

C

Gene name	Liv 1 Fc	Liv 1 Fc
Hars2	121.74	90.94
Tsnax	64.35	65.79
Cnbp	34.62	80.69
Tsn	12.54	21.39

D

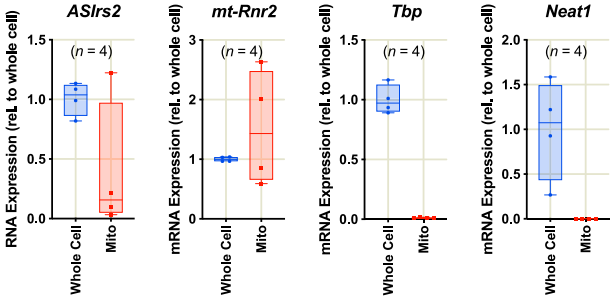

E

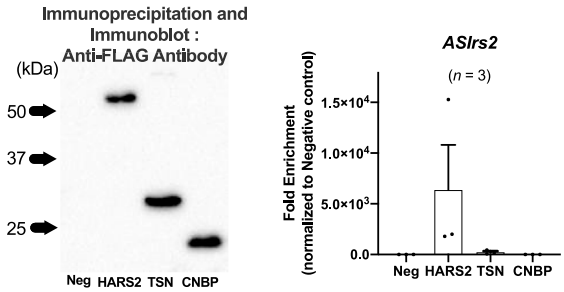

F

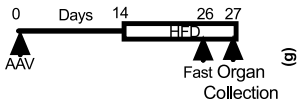

G

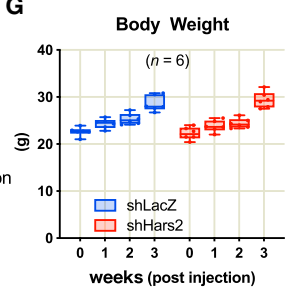

H

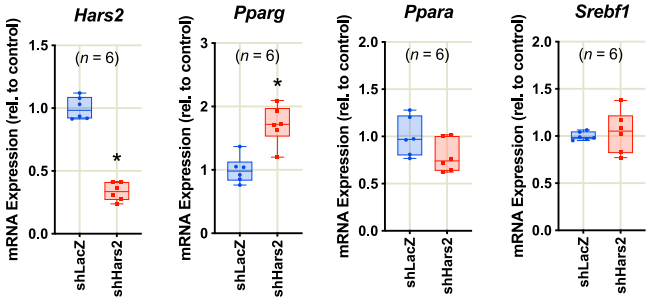

I

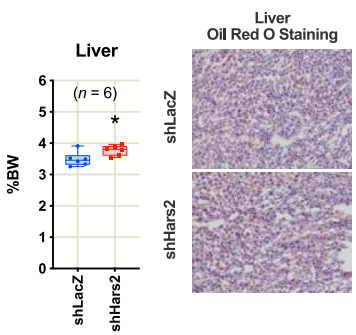

J

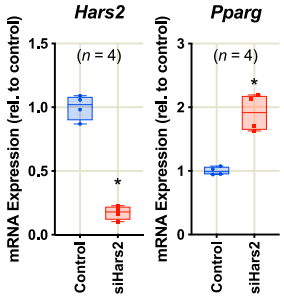

Figure 4. *ASlrs2* is bound to HARS2, the suppression of which increased hepatic *Pparg in vitro* and *in vivo*

(A) The fold enrichments of the protein amount precipitated by ASlrs2 pull-down over that precipitated by control RNA pull-down by proteomic analyses of two independent liver lysates.

(B) DAVID functional annotation analyses assessing "cellular component" of the proteins with more than 3-fold enrichment.

(C) The four proteins with the highest enrichments. Fc, fold change.

(legend continued on next page)

that *ASIrs2* and HARS2 interacted elsewhere in the cell. Second, the binding assays detecting HARS2 required overexpression of *ASIrs2* due to its low expression level, carrying a risk of detecting super-physiological interaction. Although our *in vivo* as well as our *in vitro* assessments using *ASIrs2* or *Hars2* suppression showed consistent results supporting their possible interaction, other mechanisms could exist mediating *ASIrs2* function.

Finally, we identified *AL162497.1* as a possible human ortholog for *ASIrs2*. Long ncRNAs are often poorly conserved among species, as seen in our case, while conservation of their genomic orientation is often indicative of their functional relevance (Modarresi et al., 2012; Yamanaka et al., 2015). Our data are indeed suggestive of potential roles for *AL162497.1* in NASH pathogenesis. Currently, the only available drugs for NASH treatment are the thiazolidinediones, which could, however, potentially activate PPARγ in liver. From this aspect, targeting *AL162497.1* could offer therapeutic benefits for NASH treatment by acting additively with thiazolidinediones.

SIGNIFICANCE

Pervasive transcription throughout the genome leads to simultaneous production of multiple transcripts from many gene loci, including those related to insulin signaling, whose significance, however, has not been clarified. Our approach here has identified a previously uncharacterized natural antisense transcript, *ASIrs2*, which is derived from the gene locus of *Irs2*, one of the essential mediators of insulin actions, whose transcript levels are reciprocally regulated in the liver under different nutritional statuses. Attenuation of insulin signaling under obesity is associated with higher levels of circulating fatty acid, which is taken up by the liver, leading to steatosis as a corollary, while what triggers and activates the liver lipid uptake under such conditions has been elusive. Our finding that *ASIrs2* is upregulated under *Irs2* suppression in obese liver and promotes lipid accumulation suggests a mechanism unitarily explaining the concurrent occurrence of insulin resistance and fatty liver through organized regulation of two transcripts from one gene locus.

STAR★METHODS

Detailed methods are provided in the online version of this paper and include the following:

- KEY RESOURCES TABLE
- RESOURCE AVAILABILITY
  - Lead contact
  - Materials availability
  - Data and code availability
- EXPERIMENTAL MODEL AND SUBJECT DETAILS
  - Animals
  - Characterization of human liver samples
- METHOD DETAILS
  - RNA sequencing of mouse liver
  - Quantitative real-time PCR analysis
  - Calculation of coding potential
  - Hepatocyte fractionation
  - Gene suppression by short hairpin RNA in mouse liver
  - Immunoprecipitation and immunoblotting
  - Antibodies for immunoblot
  - Cells and cell culture experiments
  - Promoter activity assay
  - Measurement of oxygen consumption rates
  - Triglyceride measurement of liver
  - Metabolic assays
  - Kupffer cell isolation
  - ASIrs2 pulldown assay
  - Proteome analysis
  - Mitochondrial isolation and RNA extraction
  - RNA immunoprecipitation assay
- QUANTIFICATION AND STATISTICAL ANALYSIS
  - Statistical analyses

SUPPLEMENTAL INFORMATION

Supplemental information can be found online at https://doi.org/10.1016/j.chembiol.2021.12.008.

AUTHOR CONTRIBUTIONS

M.M, M.A., and K.U. designed the study and wrote the manuscript. N.K. performed metabolic challenge tests for animals. Y.M.I., K.S., and J.C.B. contributed to the discussion. M.N. performed histological analyses. M.M. performed RNA sequencing. K.K. conducted AAV generation. M.B. performed the RNA quantification of human samples. M.M. and M.A. performed the experiments and analyzed and interpreted the data.

ACKNOWLEDGMENTS

We acknowledge Fumiya Takahashi and Yuko Masaki for outstanding technical assistance. M.A. gratefully acknowledges support from a Mampei-Suzuki Diabetes Foundation fellowship. The study was conducted with funding from the National Center for Global Health and Medicine (19A1005) and a Grant-in-Aid for Scientific Research (C) (19K09037).

DECLARATION OF INTERESTS

The authors declare no competing interests.

Received: March 4, 2021
Revised: October 27, 2021
Accepted: December 6, 2021
Published: January 4, 2022

(D) The RNA expression in the fractionated mitochondria compared with whole liver cells.
(E) Representative image of FLAG immunoblot and the *ASIrs2* amount immunoprecipitated by FLAG antibody in Hepa 1-6 cells overexpressed with each FLAG-tagged protein.
(F) A schema of the *Hars2* knockdown experiment.
(G–I) The body weights (G), the relative gene expression in liver (H), and the liver weights with representative oil red O-stained images of liver sections (I) of HFD-fed wild-type mice administered shHars2 or control shLacZ AAV.
(J) The relative expression of *Hars2* and *Pparg* in Hepa 1-6 cells transfected with siRNA for *Hars2* (siHars2) or negative control siRNA (Control). *$p < 0.05$ using two-tailed Student's t test. For explanation of boxplots see Figure 1 legend. See also Figure S4.

REFERENCES

Amodei, D., Egertson, J., MacLean, B.X., Johnson, R., Merrihew, G.E., Keller, A., Marsh, D., Vitek, O., Mallick, P., and MacCoss, M.J. (2019). Improving precursor selectivity in data-independent acquisition using overlapping windows. J. Am. Soc. Mass Spectrom. *30*, 669–684.

Amrutkar, M., Kern, M., Nunez-Duran, E., Stahlman, M., Cansby, E., Chursa, U., Stenfeldt, E., Boren, J., Bluher, M., and Mahlapuu, M. (2016). Protein kinase STK25 controls lipid partitioning in hepatocytes and correlates with liver fat content in humans. Diabetologia *59*, 341–353.

Brown, M.S., and Goldstein, J.L. (2008). Selective versus total insulin resistance: a pathogenic paradox. Cell Metab. *7*, 95–96.

Cho, Y.W., Hong, S., Jin, Q., Wang, L., Lee, J.E., Gavrilova, O., and Ge, K. (2009). Histone methylation regulator PTIP is required for PPARgamma and C/EBPalpha expression and adipogenesis. Cell Metab. *10*, 27–39.

Consortium, E.P., Bernstein, B.E., Birney, E., Dunham, I., Green, E.D., Gunter, C., and Snyder, M. (2012). An integrated encyclopedia of DNA elements in the human genome. Nature *489*, 57–74.

Dennis, G., Jr., Sherman, B.T., Hosack, D.A., Yang, J., Gao, W., Lane, H.C., and Lempicki, R.A. (2003). DAVID: database for annotation, visualization, and integrated discovery. Genome Biol. *4*, P3.

Donnelly, K.L., Smith, C.I., Schwarzenberg, S.J., Jessurun, J., Boldt, M.D., and Parks, E.J. (2005). Sources of fatty acids stored in liver and secreted via lipoproteins in patients with nonalcoholic fatty liver disease. J. Clin. Invest. *115*, 1343–1351.

Faghihi, M.A., and Wahlestedt, C. (2009). Regulatory roles of natural antisense transcripts. Nat. Rev. Mol. Cel. Biol. *10*, 637–643.

Gispert, S., Parganlija, D., Klinkenberg, M., Drose, S., Wittig, I., Mittelbronn, M., Grzmil, P., Koob, S., Hamann, A., Walter, M., et al. (2013). Loss of mitochondrial peptidase Clpp leads to infertility, hearing loss plus growth retardation via accumulation of CLPX, mtDNA and inflammatory factors. Hum. Mol. Genet. *22*, 4871–4887.

Grimm, D., Streetz, K.L., Jopling, C.L., Storm, T.A., Pandey, K., Davis, C.R., Marion, P., Salazar, F., and Kay, M.A. (2006). Fatality in mice due to oversaturation of cellular microRNA/short hairpin RNA pathways. Nature *441*, 537–541.

Guo, M., and Schimmel, P. (2013). Essential nontranslational functions of tRNA synthetases. Nat. Chem. Biol. *9*, 145–153.

Huang, D., Chen, J., Yang, L., Ouyang, Q., Li, J., Lao, L., Zhao, J., Liu, J., Lu, Y., Xing, Y., et al. (2018). NKILA lncRNA promotes tumor immune evasion by sensitizing T cells to activation-induced cell death. Nat. Immunol. *19*, 1112–1125.

Jump, D.B., Botolin, D., Wang, Y., Xu, J., Christian, B., and Demeure, O. (2005). Fatty acid regulation of hepatic gene transcription. J. Nutr. *135*, 2503–2506.

Katayama, S., Tomaru, Y., Kasukawa, T., Waki, K., Nakanishi, M., Nakamura, M., Nishida, H., Yap, C.C., Suzuki, M., Kawai, J., et al. (2005). Antisense transcription in the mammalian transcriptome. Science *309*, 1564–1566.

Kawashima, Y., Watanabe, E., Umeyama, T., Nakajima, D., Hattori, M., Honda, K., and Ohara, O. (2019). Optimization of data-independent acquisition mass spectrometry for deep and highly sensitive proteomic analysis. Int. J. Mol. Sci. *20*, 5932.

Kong, L., Zhang, Y., Ye, Z.Q., Liu, X.Q., Zhao, S.Q., Wei, L., and Gao, G. (2007). CPC: assess the protein-coding potential of transcripts using sequence features and support vector machine. Nucleic Acids Res. *35*, W345–W349.

Kubota, N., Kubota, T., Itoh, S., Kumagai, H., Kozono, H., Takamoto, I., Mineyama, T., Ogata, H., Tokuyama, K., Ohsugi, M., et al. (2008). Dynamic functional relay between insulin receptor substrate 1 and 2 in hepatic insulin signaling during fasting and feeding. Cell Metab. *8*, 49–64.

Kubota, N., Kubota, T., Kajiwara, E., Iwamura, T., Kumagai, H., Watanabe, T., Inoue, M., Takamoto, I., Sasako, T., Kumagai, K., et al. (2016). Differential hepatic distribution of insulin receptor substrates causes selective insulin resistance in diabetes and obesity. Nat. Commun. *7*, 12977.

Lee, Y.K., Park, J.E., Lee, M., and Hardwick, J.P. (2018). Hepatic lipid homeostasis by peroxisome proliferator-activated receptor gamma 2. Liver Res. *2*, 209–215.

Lin, S., Zhang, L., Luo, W., and Zhang, X. (2015). Characteristics of antisense transcript promoters and the regulation of their activity. Int. J. Mol. Sci. *17*, 9.

Matsuo, K., Matsusue, K., Aibara, D., Takiguchi, S., Gonzalez, F.J., and Yamano, S. (2017). Insulin represses fasting-induced expression of hepatic fat-specific protein 27. Biol. Pharm. Bull *40*, 888–893.

Matsusue, K., Haluzik, M., Lambert, G., Yim, S.H., Gavrilova, O., Ward, J.M., Brewer, B., Jr., Reitman, M.L., and Gonzalez, F.J. (2003). Liver-specific disruption of PPARgamma in leptin-deficient mice improves fatty liver but aggravates diabetic phenotypes. J. Clin. Invest. *111*, 737–747.

Mercer, T.R., Neph, S., Dinger, M.E., Crawford, J., Smith, M.A., Shearwood, A.M., Haugen, E., Bracken, C.P., Rackham, O., Stamatoyannopoulos, J.A., et al. (2011). The human mitochondrial transcriptome. Cell *146*, 645–658.

Modarresi, F., Faghihi, M.A., Lopez-Toledano, M.A., Fatemi, R.P., Magistri, M., Brothers, S.P., van der Brug, M.P., and Wahlestedt, C. (2012). Inhibition of natural antisense transcripts in vivo results in gene-specific transcriptional upregulation. Nat. Biotechnol. *30*, 453–459.

Moran-Salvador, E., Lopez-Parra, M., Garcia-Alonso, V., Titos, E., Martinez-Clemente, M., Gonzalez-Periz, A., Lopez-Vicario, C., Barak, Y., Arroyo, V., and Claria, J. (2011). Role for PPARgamma in obesity-induced hepatic steatosis as determined by hepatocyte- and macrophage-specific conditional knockouts. FASEB J. *25*, 2538–2550.

Muppirala, U.K., Honavar, V.G., and Dobbs, D. (2011). Predicting RNA-protein interactions using only sequence information. BMC Bioinformatics *12*, 489.

Newman, W.G., Friedman, T.B., Conway, G.S., and Demain, L.A.M. (1993). Perrault syndrome. In GeneReviews, M.P. Adam, H.H. Ardinger, R.A. Pagon, S.E. Wallace, L.J.H. Bean, K. Stephens, and A. Amemiya, eds. (Seattle), pp. 1–19.

Noh, J.H., Kim, K.M., Abdelmohsen, K., Yoon, J.H., Panda, A.C., Munk, R., Kim, J., Curtis, J., Moad, C.A., Wohler, C.M., et al. (2016). HuR and GRSF1 modulate the nuclear export and mitochondrial localization of the lncRNA RMRP. Genes Dev. *30*, 1224–1239.

Ozsolak, F., Kapranov, P., Foissac, S., Kim, S.W., Fishilevich, E., Monaghan, A.P., John, B., and Milos, P.M. (2010). Comprehensive polyadenylation site maps in yeast and human reveal pervasive alternative polyadenylation. Cell *143*, 1018–1029.

Palazzo, A.F., and Koonin, E.V. (2020). Functional long non-coding RNAs evolve from junk transcripts. Cell *183*, 1151–1161.

Pelechano, V., and Steinmetz, L.M. (2013). Gene regulation by antisense transcription. Nat. Rev. Genet. *14*, 880–893.

Searle, B.C., Pino, L.K., Egertson, J.D., Ting, Y.S., Lawrence, R.T., MacLean, B.X., Villen, J., and MacCoss, M.J. (2018). Chromatogram libraries improve peptide detection and quantification by data independent acquisition mass spectrometry. Nat. Commun. *9*, 5128.

Shimomura, I., Matsuda, M., Hammer, R.E., Bashmakov, Y., Brown, M.S., and Goldstein, J.L. (2000). Decreased IRS-2 and increased SREBP-1c lead to mixed insulin resistance and sensitivity in livers of lipodystrophic and ob/ob mice. Mol. Cell *6*, 77–86.

Wang, L., Park, H.J., Dasari, S., Wang, S., Kocher, J.P., and Li, W. (2013). CPAT: coding-potential assessment tool using an alignment-free logistic regression model. Nucleic Acids Res. *41*, e74.

Wang, M., Sips, P., Khin, E., Rotival, M., Sun, X., Ahmed, R., Widjaja, A.A., Schafer, S., Yusoff, P., Choksi, P.K., et al. (2016). Wars2 is a determinant of angiogenesis. Nat. Commun. *7*, 12061.

Wang, Y., Nakajima, T., Gonzalez, F.J., and Tanaka, N. (2020). PPARs as metabolic regulators in the liver: lessons from liver-specific PPAR-null mice. Int. J. Mol. Sci. *21*, 2061.

Xia, P., Wang, S., Ye, B., Du, Y., Li, C., Xiong, Z., Qu, Y., and Fan, Z. (2018). A circular RNA protects dormant hematopoietic stem cells from DNA sensor cGAS-mediated exhaustion. Immunity *48*, 688–701 e687.

Yamanaka, Y., Faghihi, M.A., Magistri, M., Alvarez-Garcia, O., Lotz, M., and Wahlestedt, C. (2015). Antisense RNA controls LRP1 Sense transcript expression through interaction with a chromatin-associated protein, HMGB2. Cell Rep. *11*, 967–976.

STAR★METHODS

KEY RESOURCES TABLE

REAGENT or RESOURCE	SOURCE	IDENTIFIER
Antibodies		
Anti-IRS2	Santa Cruz	Cat# sc-8299; RRID: AB_2125783
Anti-IRS2	Sigma-Aldrich	Cat# MABS15; RRID: AB_10615782
Anti-phospho Akt (Ser473)	Cell Signaling	Cat# 4060; RRID: AB_2315049
Anti-Akt	Cell Signaling	Cat# 4691; RRID: AB_915783
Anti-FLAG® M2	Sigma-Aldrich	Cat# F1804; RRID: AB_262044
Anti-Rabbit IgG-Peroxidase	Sigma-Aldrich	Cat# A6154; RRID: AB_258284
Anti-Mouse IgG-Peroxidase	Sigma-Aldrich	Cat# A4416; RRID: AB_258167
Bacterial and virus strains		
AAV/DJ8 shASIrs2	Vector Biolabs	NA
AAV/DJ8 shHars2	National Institute for Physiological Sciences	NA
LNA GapmeR for ASIrs2	This paper, from QIAGEN	NA
LNA GapmeR Negative Control A	QIAGEN	LG00000002-DDA
Chemicals, peptides, and recombinant proteins		
High Fat Diet (60% kcal Fat)	JAPAN CLEA	HFD32
Collagenase Type IV	Worthington	CLS-4
Histodenz®	Sigma-Aldrich	D2158
Percoll®	GE Healthcare	17-0891-02
Dynabeads® Protein G	ThermoFisher Scientific	DB10004
Critical commercial assays		
RiboTrap Kit	MBL	RN1011
Riboprobe In Vitro Transcription System	Promega	P1430, P1440
Mitochondria Isolation Kit	101Bio	(Discontinued)
Deposited data		
Un-cropped images of immunoblots	This paper	https://data.mendeley.com/datasets/vd88zjfvbr/3
RNAseq data of liver from obese mouse models	This paper	GSE188344
RNAseq data of liver from shASIrs2-AAV treated mice	This paper	GSE188428
Experimental models: Cell lines		
Hepa 1–6 cells	ATCC	CRL-1830
Experimental models: Organisms/strains		
Mouse/C57BL6/N	Japan CLEA	NA
Mouse/BKS.Cg-Dock7m +/+ Leprdb/J	Japan CLEA	NA
Oligonucleotides		
Pparg1 Forward: AAAGAAGCGGTGAA CCACTGATA	(Cho et al., 2009)	NA
Pparg1 Reverse: AATGGCATCTCTGTG TCAACCA	(Cho et al., 2009)	NA
Pparg1 Probe: ACCCTTTACTGAAATTACC	(Cho et al., 2009)	NA
Pparg2 Forward: CGCTGATGCACTGCCT ATGA	(Cho et al., 2009)	NA
Pparg2 Reverse: AATGGCATCTCTGTGTC AACCA	(Cho et al., 2009)	NA

(*Continued on next page*)

Continued

REAGENT or RESOURCE	SOURCE	IDENTIFIER
Pparg2 Probe: CACTTCACAAGAAATTAC	(Cho et al., 2009)	NA
Taqman probe for *AL162497.1*	This paper, from ThermoFisher Scientific	NA
Recombinant DNA		
Hars2 (NM_080636) Mouse Tagged ORF Clone	ORIGENE	MR208134
Cnbp (NM_013493) Mouse Tagged ORF Clone	ORIGENE	MR201568
Tsn (NM_011650) Mouse Tagged ORF Clone	ORIGENE	MR202740
Software and algorithms		
Coding-potential Assessment Tool	(Wang et al., 2013)	http://lilab.research.bcm.edu/
Coding Potential Calculator	(Kong et al., 2007)	http://cpc2.gao-lab.org/
GraphPad PRISM 8	GraphPad Software	www.graphpad.com

RESOURCE AVAILABILITY

Lead contact

Further information and requests for resources and reagents are directed to and handled by the lead contact Motoharu Awazawa (mawazawa@ri.ncgm.go.jp).

Materials availability

This study did not generate new unique reagents.

Data and code availability

RNAseq data are deposited at GEO and are publicly available as of the date of publication. Accession numbers are listed in the key resources table.

This paper does not include any original code.

Any additional information required to reanalyze the data reported in this paper is available from the lead contact upon request.

EXPERIMENTAL MODEL AND SUBJECT DETAILS

Animals

C57BL/6 wild-type male mice and *BKS.Cg-Dock7m* +/+ Leprdb/J (*db/db*) male mice or their control *misty/misty* male mice, the littermates of *db/db* mice generated on the *BKS.Cg-Dock7m* +/+ *Lepr*^{db}/J background, were purchased from Japan CLEA. Mice were housed at 22°C in a 12-hour-12-hour light-dark cycle and fed a standard rodent normal chow diet (CE-2, Japan CLEA; Harlan) unless otherwise indicated. For the assessment of differently regulated genes in liver under obesity, *C57BL/6* wild-type male mice were fed on high-fat diet (HFD32, 60% kcal from fat; Japan CLEA) or a low-fat diet (CE-2, 4.51% kcal from fat; Japan CLEA) for 18 weeks starting from 6 weeks of age, and the livers were collected at 24 weeks of age at a*d libitum*-fed condition. In the fasting-refeeding regimen, the mice were fasted for 20 hours, with or without additional 6 hours of refeeding, prior to organ collection. For the analysis of pooled liver samples, the liver from *C57BL6* mice fed with HFD for 6, 12 or 18 weeks from 6 weeks of age (n = 6 each), *db/db* mice at 10 weeks of age (n = 5 each) and their respective control mice were pooled and subjected to the analysis. All the animals were randomly assigned to the experimental groups and the tests were done in a blinded way. Sample sizes for animal experiments were calculated based on power calculations with an alpha of 0.8. All the animal care and experimentation procedures were approved by the Animal Care and Use Committee of the National Center for Global Health and Medicine abiding by ethical guidelines.

Characterization of human liver samples

The *AL162497.1* and *PPARG* mRNA expression were measured in liver tissue samples obtained from 33 human subjects who underwent open abdominal surgery for Roux-en-Y bypass, sleeve gastrectomy, explorative laparotomy or elective cholecystectomy (Table S1). The study was approved by the Ethics Committee of the University of Leipzig (approval numbers: 363-10-13122010 159-12-21052012), and performed in accordance to the declaration of Helsinki. All subjects gave written informed consent to use their data in anonymized form for research purposes before taking part in this study. A small liver biopsy was taken during the surgery, immediately snap-frozen in liquid nitrogen, and stored at −80°C until further preparations. All baseline blood samples and liver biopsies were collected between 8:00 hours and 10:00 hours after an overnight fast. Liver biopsy donors fulfilled the following inclusion

criteria: (1) men and women, age >18 years; (2) indication for elective laparoscopic or open abdominal surgery; (3) BMI between 18 and 50 kg/m2; (4) abdominal MRI feasible; and (5) signed written informed consent. The exclusion criteria were: (1) significant acute or chronic inflammatory disease or clinical signs of infection; (2) C-reactive protein (CrP) >952.4 nmol/l; (3) type 1 diabetes and/or antibodies against GAD and islet cell antibodies (ICA); (4) systolic blood pressure >140 mmHg and diastolic blood pressure >95 mmHg; (5) clinical evidence of either cardiovascular or peripheral artery disease; (6) thyroid dysfunction; (7) alcohol or drug abuse; and (8) pregnancy (Amrutkar et al., 2016). The RNA expression in human liver was measured by quantitative real-time PCR in a fluorescent temperature cycler ABI PRISM 7000 sequence detector (Applied Biosystems, Darmstadt, Germany). The probe detecting *AL162497.1* was designed with the targeted sequence GAC-CCC-TCT-AGA-TCA-AGT-TTG-CAA-A in the exon junction and provided by Applied Biosystems. The mRNA expression was calculated relative to the mRNA expression of *Hypoxanthin-Guanin-Phosphoribosyltransferase 1* (*HPRT1*) (Hs01003267_m1; Applied Biosystems, Darmstadt, Germany).

METHOD DETAILS

RNA sequencing of mouse liver

Total RNA was isolated from liver using TRIZOL reagent (Invitrogen). The sample RNA concentration was measured by Nanodrop 2000 (ThermoFisher) and the RNA quality was assessed by RNA 6000 Pico kit (Agilent). 200 ng of total RNA was used for RNA-sequencing library preparation with NEB NEBNext rRNA Depletion Kit and NEBNext Ultra Directional RNA Library Prep Kit (New England Biolabs). Library size and concentration were verified with High-sensitivity DNA Kit (Agilent). Sequencing was performed with NextSeq500 (Illumina) to obtain 2 × 36 base paired-end reads. FASTQ files were imported to CLC Genomics Workbench (CLC-GW, Version 10.1.1, Qiagen). Reads were mapped to mouse reference genome (mm10) and quantified for annotated 49,585-gene set provided by CLC-GW.

Quantitative real-time PCR analysis

Total RNA was extracted from the tissues using Tissue Total RNA Mini Kit (FAVORGEN). cDNA was synthesized by reverse transcription using High-capacity cDNA Reverse Transcription Kit (ThermoFisher). Quantitative real-time PCR analyses were performed using StepOnePlus™ Real Time PCR System (Applied Biosystems) with KAPA PROBE FAST qPCR Master Mix (2X) kit (Kapa Biosystems). The relative gene expression was calculated by a comparative method using the values normalized to that of *Tbp* or *Hprt* in the same sample as the internal control gene expression, except for miR-122 quantification in liver samples where that of sno429 expression was used for normalization. For specific quantification of *Pparg1* and *Pparg2*, the following oligonucleotides were synthesized by ABI (Cho et al., 2009): For *Pparg1*, Probe: ACCCTTTACTGAAATTACC, Forward Primer: AAAGAAGCGGTGAACCACTGATA, Reverse Primer: AATGGCATCTCTGTGTCAACCA; For *Pparg2*, Probe: CACTTCACAAGAAATTAC, Forward Primer: CGCTGATGCACTGCCTATGA, Reverse Primer: AATGGCATCTCTGTGTCAACCA. Otherwise, all the primers and probes were purchased from Applied Biosystems (ABI).

Calculation of coding potential

The coding-potential of *ASIrs2* transcript was calculated by two independent web-based programs; Coding-potential Assessment Tool (CPAT (Wang et al., 2013)) and Coding Potential Calculator (CPC (Kong et al., 2007)). The results of coding potential for the well-established ncRNAs such as *Xist*, *Tsix* and *Hotair* as well as those for canonical coding gene such as *Gapdh*, *Pck1* and *Acta2* were plotted together with the results for *ASIrs2* and *Irs2*.

Hepatocyte fractionation

C57BL/6 male mice were used for primary liver cell isolation at around 8 weeks of age. Under anesthesia, the mice were perfused via the portal vein with 50 ml of Hank's buffered salt solution without magnesium or calcium (Sigma) supplemented with 0.5mM EGTA (perfusion medium), and subsequently perfused with 50 ml of Dulbecco's Modified Eagle's Medium (DMEM)-low glucose (Gibco) supplemented with 15 mM HEPES and 100 CDU/ml of Collagenase Type IV (Worthington) (digestion medium). After perfusion, the liver capsule was carefully removed and the dissociated cells were collected through a Cell Strainer (100 μm, BD Falcon) into DMEM-low glucose (Gibco) supplemented with 10% fetal bovine serum. For the fractionation of hepatocytes and non-parenchymal cells, the total liver cells were first centrifuged at 50 g for 3 minutes. The supernatant was centrifuged at 350 g, and the cell pellet was centrifuged on a 20% (wt/vol) Histodenz (Sigma) gradient for non-parenchymal cell purification. The pellet of the first centrifugation was re-suspended in 30% Percoll and centrifuged at 150 g for 7 minutes for hepatocyte purification. Each fraction was subjected to RNA extraction. Subsequently, for subcellular fractionation of hepatocytes, the purified hepatocytes were subjected to fractionation using Cytoplasmic and Nuclear RNA Purification Kit (Norgen Biotek) following the manufacture's protocol.

Gene suppression by short hairpin RNA in mouse liver

AAV serotype DJ8 (AAV/DJ8) encoding an shRNA sequence targeting *ASIrs2* (Vector Biolabs) or *Hars2* (produced by K.K.) and the control shRNA sequence were produced. The shRNA constructs were inserted in the vector under the control of U6 promoter. The targeting siRNA sequence for *ASIrs2* was CUU-ACA-GAA-GGA-CAG-ACA-AUA, which we designed to target lower exon of *ASIrs2*, so that it would not interfere with the expression of overlapping *Irs2*. The control AAV carrying a scrambled shRNA construct was purchased from Vector Biolabs. The targeting siRNA sequence for *Hars2* was GGG-AGA-AAA-UCC-UCG-AUA-A. The control

AAV carrying a shRNA construct against LacZ was produced by K. K. For the *ASIrs2*-knockdown experiment using *misty*/*misty* or *db*/*db mice*, the mice were injected with the AAV via tail vein at the titer of 5×10^{11} particles/animal at 8 weeks of age. The insulin tolerance test was performed at 17 days, and the glucose tolerance test was performed at 22 days after AAV injection. The mice were sacrificed for organ collection at the fasted status on the 27th or 28th day after AAV injection. For the *ASIrs2*-knockdown experiment using *C57BL/6* mice, the mice were injected with the AAV via tail vein at the titer of 2×10^{11} particles/animal at 8 weeks of age, and the mice were sacrificed for organ collection at the fasted status or after subsequent refeeding for 6 hours on the 27th or 28th day after AAV injection. For the Hars2-knockdown experiment, the mice were injected with the AAV via tail vein at the titer of 1.5×10^{11} particles/animal at 8 weeks of age, high-fat-diet feeding was started two weeks after AAV injection and the mice were sacrificed for organ collection at the fasted status on the 27th day after AAV injection.

Immunoprecipitation and immunoblotting

The tissues were homogenized in ice cold Liver Buffer (25 mM Tris-HCl, pH 7.4, 10 mM Na_3VO_4, 100 mM NaF, 50 mM Na_4P2O_7, 10 mM EGTA, and 10 mM EDTA) with 1% Nonidet-P 40, supplemented with cOmplete Mini Protease Inhibitor Cocktail (Roche). After homogenization, the lysate was centrifuged at 55000 rpm for 60 minutes at 4°C and the supernatant was collected. The protein concentration of lysate was determined by BCA Assay Kit (ThermoFisher). For immunoprecipitation, 3 mg of liver protein lysate was incubated with 2 μg of antibody for two hours at 4°C with gentle rotation. Subsequently, the immunocomplex was collected by incubating the precipitates with Dynabeads (ThermoFisher) for 30 minutes at 4°C. For sample preparation, the immunoprecipitants were heated at 95°C for 5 minutes in Laemmli buffer. The prepared samples were subjected to SDS-PAGE, followed by an electrical transfer to PVDF membrane in Trans-Blot TURBO system (BIO-RAD). After blocking with skim milk, the membrane was incubated with the primary antibodies at 4°C overnight. Subsequently after incubation with the secondary antibody for one hour at room temperature, the blot was developed using Pierce ECL Western Blotting Substrate (ThermoFisher). For the quantitative analyses, the densitometry was performed with the Fiji image processing package. The files of un-cropped images of immunoblots are deposited in Mendeley (https://data.mendeley.com/datasets/vd88zjfvbr/3).

Antibodies for immunoblot

The antibody against IRS-2 (sc-8299, SantaCruz) was used for immunoprecipitation, and the antibody against IRS-2 (MABS15, Sigma-Aldrich) was used for immunoblot at 1:1000 dilution. The antibodies against phosphorylated Akt (S473: #4060) and total Akt (#4691) were purchased from Cell Signaling. For the immunoblot with total Akt, the membrane blotted with the phosphorylated Akt antibody was re-probed with the total Akt antibody. Anti-FLAG® M2 Antibody was purchased from Sigma and used for immunoblot at 1:5000 dilution. The secondary antibody Anti-Rabbit IgG-Peroxidase antibody (A6154) or Anti-Mouse IgG-Peroxidase antibody (A4416) was purchased from Sigma-Aldrich and used at 1:5000 dilution.

Cells and cell culture experiments

Hepa 1-6 cells were cultured in DMEM (High glucose) medium supplemented with penicillin and streptomycin and 10% fetal bovine serum. The cells were originally derived from American Type Culture Collection (ATCC), and tested negative for mycoplasma contamination. All the cell culture experiments were conducted without blinding. For siRNA- or LNA-mediated gene suppression, the cells were plated at the density of 0.5×10^5 cells/well in 24 well plates one day prior to the transfection. On the following day, siRNA or LNA was transfected with Lipofectamine RNAi max following the manufacture's protocol, and the cells were collected for RNA extraction at 48 hours post transfection. The final siRNA concentrations used were 40 nM for the *Hars2* suppression experiment and 150 nM for the *ASIrs2* suppression experiment. The siRNA sequence was: siASIrs2 CUU-ACA-GAA-GGA-CAG-ACA-AUA; siHars2 GGG-AGA-AAA-UCC-UCG-AUA-A. Universal Negative Control siRNA was purchased from Nippon Gene and used as the negative control with the same concentration as above. For the LNA using experiment, the final LNA concentration was 150 nM, and the LNA sequence was ACT-GGA-ATC-ATC-TGC-A which was synthesized and purchased from QIAGEN together with Negative Control A: AAC-ACG-TCT-ATA-CGC as the negative control. For the analyses, the numbers of replicates were counted as the number of independently repeated experiments, with the values being normalized to the first well of the control samples in each experiment. Two to four wells were analyzed for each replicate.

Promoter activity assay

3.1 kbp of 5'-flanking region of mouse *Pparg1* gene was synthesized by Thermofisher Scientific and was subcloned into pGL3 vector (Promega). Hepa 1-6 cells were plated onto a 24-well plate at a cell density of 5×10^4 cells/well, and 300 ng of the luciferase reporter plasmid and 20 ng of a Renilla luciferase plasmid (pRL-null, Promega) were co-transfected with siRNA at a final concentration of 240 nM by Lipofectamine 2000 (Life Technologies). At 48 hours post transfection, the cells were harvested and subjected to luciferase assays using Dual-Luciferase Reporter Assay System (Promega) following the manufacturer's protocol. When applicable, the cells were stimulated with recombinant human insulin at 10nM for 24 hours before collection.

Measurement of oxygen consumption rates

Oxygen consumption rate (OCR) of Hepa 1-6 cells with siRNA-mediated gene suppression was measured using the Seahorse Flux Analyzer XF24 (Agilent). The cells were transfected with 120 nM of siASIrs2 or control siRNA in DMEM (High glucose) medium supplemented with penicillin and streptomycin and 10% fetal bovine serum. 48 hours later, the medium was changed to XF Base Medium

(Agilent) supplemented with 25 mM of glucose, 4 mM of glutamine and 1mM of sodium pyruvate (Agilent), and OCR measurement was conducted with subsequent stimulation by 1.5 μM oligomycin, 0.5 μM fluoro-carbonyl cyanide phenylhydrazone (FCCP) and 0.5 μM Rotenone/Antimycin A (Seahorse XF Cell Mito Stress Test Kit, Agilent) according to the manufacture's protocol.

Triglyceride measurement of liver

Around 100 mg of freshly frozen liver pieces were completely digested with 1700 μl of ethanolic KOH (EtOH:30% KOH = 2:1) for overnight at 55°C with vigorous shaking. 200 μl of the lysate was mixed with 215 μl of 1M MgCl2, and after incubation on ice for 5 minutes, was centrifuged. The supernatant was subjected to the triglyceride measurement using Triglyceride-E Test kit (WAKO).

Metabolic assays

For the insulin tolerance test, the mice were injected with 2.5 i.U./kg body weight of insulin (Humalin R, Eli-Lilly Japan) intraperitoneally at ad libitum status. For the glucose tolerance test, the mice were injected with 1 g/kg body weight of glucose intraperitoneally after fasting for 16 hours. The blood samples were collected at indicated time points and the blood glucose levels were determined by Glutest Mint (Sanwa Kagaku Kenkyusho), which allowed measurement of blood glucose levels up to 1000 mg/dl. Plasma insulin levels were measured using Mouse Insulin ELISA Kit (Morinaga Institute of Biological Science).

Kupffer cell isolation

The freshly collected liver was minced and digested with Liver Dissociation Kit (Miltenyi Biotec) according to the manufacture's instruction. After tissue digestion, cells were passed through a 70 mm cell strainer, and hepatocytes were removed by two low-speed centrifugation steps at 50 g for 2 minutes. Non-parenchymal cells (NPCs) in the supernatant were further separated from debris by pelleting for 30 minutes at 3,000 g in Debris Removal Solution (Miltenyi Biotec) at 4°C. Subsequently, the cells were resuspended with 30% iodixanol solution (Optiprep, Axis-Shield, Oslo, Norway) and carefully underlaid beneath Gey's Balanced Salt Solution (GBSS). The resulting gradient was centrifuged at 1,400 G for 21 minutes at 4°C with no brake and the cells enriched at the interface were collected. After being washed, the enriched NPCs were stained in wash buffer with anti-CD11b antibody-conjugated magnetic beads (Miltenyi Biotec) for 15 minutes at 4°C. Labeled cells were enriched using magnetic columns and collected as Kupffer cells.

ASIrs2 pulldown assay

ASIrs2 pulldown assay was conducted using RiboTrap Kit (MBL) according to the manufacture's protocol. Briefly, BromoUTP-labelled *ASIrs2* RNA was synthesized by *in vitro* transcription of a plasmid using Riboprobe In Vitro Transcription System (Promega). The RNA transcribed from the same plasmid using a reverse promoter, i.e. the reverse transcript for *ASIrs2*, was also synthesized and used as the control RNA. The synthesized RNA was purified with MEGA Clear Transcription Clean-Up Kit (ThermoFisher) after DNAse digestion (Qiagen). Liver lysates were prepared from primary hepatocytes isolated from *db/db* mouse under fasting for overnight according to the manufacture's protocol. The nuclear fraction and cytosolic fraction were pooled and subjected to the further processes. The synthesized RNA was bound to the anti-BrU antibody-conjugated beads, and then incubated with the liver lysates for two hours at 4 degree for immunoprecipitation. Subsequently the immunoprecipitated conjugates were collected, washed with Wash Buffer I and eluted by incubation with excessive amount of BrdU for 30 minutes. The eluates were directly subjected to proteome analysis.

Proteome analysis

The pretreatments of shotgun proteome analysis such as reduction and alkylation of cysteine residues and enzymatic digestion were performed as previously reported (Kawashima et al., 2019). Namely, the protein was treated with 10 mM dithiothreitol at 50°C for 30 min and then subjected to alkylation with 30 mM iodoacetamide in the dark at room temperature for 30 min. The reaction of iodoacetamide was stopped with 60 mM cysteine for 10 min. The mixture was diluted with 50 mM ammonium bicarbonate and digested by adding 1 μg of Trypsin/Lys-C mix (Promega, Madison, WI, USA) overnight at 37°C. The digested sample was acidified with 5% TFA, followed by sonication on the high setting for 5 min in 30 s on/30 s off cycles (Bioruptor UCD-200; Cosmobio Co., Tokyo, Japan). The mixture was shaken for 5 min and centrifuged at 15,000× g for 5 min. The supernatant was desalted by using C18-StageTips, followed by drying with a centrifugal evaporator. The dried peptides were redissolved in 3% ACN and 0.1% formic acid. Next, peptides were directly injected onto a 75 μm × 25 cm PicoFrit emitter (New Objective) packed in-house with C18 core-shell particles (CAPCELL CORE MP 2.7 μm, 160 Å material; Osaka Soda Co., Ltd.) at 45°C and then separated with a 90 min gradient at a flow rate of 100 nl/min using an UltiMate 3000 RSLCnano LC system (ThermoFisher). Peptides eluting from the column were analyzed on a Q Exactive HF-X (ThermoFisher) for overlapping window DIA-MS (Amodei et al., 2019; Kawashima et al., 2019). MS1 spectra were collected in the range of 495-785 m/z at 30,000 resolution to set an automatic gain control target of 3e6 and maximum injection time of 55 ms. MS2 spectra were collected in the range of more than 200 m/z at 30,000 resolution to set an automatic gain control target of 3e6, maximum injection time of "auto", and stepped normalized collision energy of 22, 26, and 30 eV. An isolation width for MS2 was set to 4 m/z and overlapping window patterns in 500-780 m/z were used window placements optimized by Skyline. MS files were searched against the mouse UniProt reference proteome (UniProt id UP000000589, reviewed, canonical) using Scaffold DIA (Proteome Software). The Scaffold DIA search parameters were as follows: experimental data search enzyme, trypsin; maximum missed cleavage sites, 1; precursor mass tolerance, 6 ppm; fragment mass tolerance, 8 ppm; static modification, cysteine carbamidomethylation. The protein identification threshold was set both peptide and protein false discovery rates of less

than 1%. Peptide quantification was calculated by EncyclopeDIA algorithm (Searle et al., 2018) in Scaffold DIA. For each peptide, the four highest quality fragment ions were selected for quantitation. Protein quantification was estimated from the summed peptide quantification.

Mitochondrial isolation and RNA extraction

Mitochondria were isolated from *C57BL/6* wild type mouse liver in *ad lib*-fed status using Mitochondria Isolation Kit (101Bio) according to the manufacture's protocol. Briefly, a freshly collected liver piece of 30 - 40 μg was homogenized in 250 μl of Lysis Buffer A on the filter column for 1 minute. Then the lysate was filtered with the column by centrifugation, from which the pellet was subjected to mitochondrial isolation according to the manufacture's protocol. The isolated mitochondria were directly subjected to RNA extraction using Tissue Total RNA Mini Kit (FAVORGEN).

RNA immunoprecipitation assay

FLAG-tagged expression vectors for *Hars2* (MR208134), *Cnbp* (MR201568) and *Tsn* (MR202740) were purchased from ORIGENE. Hepa 1-6 cells were plated in 6 well plates at the cell density of 2×10^5 cells / well. On the following day, the cells were transfected with 2.5 μg of the respective expression plasmid or a negative control empty vector. 72 hours after transfection, the cells were collected in 1ml of cell lysis buffer (20 mM HEPES, pH 7.5, 150 mM NaCl, 50 mM NaF, 1 mM Na_3VO_4, 1% digitonin, 1 mM $MgCl_2$) supplemented with cOmplete Mini Protease Inhibitor Cocktail (Roche). Cells were immediately centrifuged at 15000 rpm for 10 minutes, and the lysates were collected. For the antibody-conjugated beads preparation, 5 μg Flag-M2-antibody (Sigma-Aldrich) was incubated with 30 μl of Dynabeads Protein G (ThermoFisher) in 800 μl of wash buffer (10 mM HEPES, pH 7.5, 150 mM NaCl, 0.1% Triton X-100) by rotating the tubes for 30 minutes at room temperature. Subsequently, the prepared lysates were incubated with the antibody-conjugated beads by rotating the tubes at 4 degree for 1 hour. After washing the beads with the wash buffer for three times, the precipitated proteins were eluted with incubating the beads with 120 μl of elution buffer (0.5 mg/ml FLAG peptide (Sigma-Aldrich) dissolved in wash buffer) by incubating the tubes on ice for 5 minutes. The resultant supernatant was subjected to RNA extraction and quantitative RT-PCR analyses, or directly to immunoblot for FLAG expression with the same antibody. The replicates were counted as the number of independently repeated experiments, with the experimental values being normalized to the average of the control samples in each experiment.

QUANTIFICATION AND STATISTICAL ANALYSIS

Statistical analyses

All the analyses were performed with GraphPad PRISM 8. Unless otherwise specified, data sets were analyzed for statistical significance using Unpaired, Two-tailed Student's *t*-test or One-way ANOVA with the Holm-Sidak multiple comparison test. In the liver triglyceride measurement, one outlier was detected by ROUT method with Q = 1% cut-off and was excluded from the analyses (Figure 3P). In the statistical correlation analyses for the human data, winsorization was applied, with the outliers detected by ROUT method with Q = 1% cut-off being substituted with the highest value in the remaining data. The distribution normality was tested by D'Agostino and Pearson test before applying a parametric correlation. For comparison of multiple groups of human subjects, Kruskal-Wallis test with Dunn's multiple comparison correction was applied as distribution normality was not guaranteed by D'Agostino-Pearson test.